ORIGINAL ARTICLE

Dynamic modulation of theta–gamma coupling during rapid eye movement sleep

Mojtaba Bandarabadi[1,2], Richard Boyce[3], Carolina Gutierrez Herrera[1,2], Claudio L. Bassetti[1,2], Sylvain Williams[3], Kaspar Schindler[1,2,4] and Antoine Adamantidis[1,2,4,*]

[1]Center for Experimental Neurology, Department of Neurology, Inselspital University Hospital, University of Bern, Bern, [2]Department for BioMedical Research, University of Bern, Bern, Switzerland and [3]Department of Psychiatry, McGill University, Montreal, Quebec, Canada

[4]Co-last authors.

*Corresponding author: Antoine Adamantidis, Department of Neurology, Inselspital University Hospital, University of Bern, Freiburgstrasse 18, 3010 Bern, Switzerland. Email: antoine.adamantidis@dbmr.unibe.ch.

Abstract

Theta phase modulates gamma amplitude in hippocampal networks during spatial navigation and rapid eye movement (REM) sleep. This cross-frequency coupling has been linked to working memory and spatial memory consolidation; however, its spatial and temporal dynamics remains unclear. Here, we first investigate the dynamics of theta–gamma interactions using multiple frequency and temporal scales in simultaneous recordings from hippocampal CA3, CA1, subiculum, and parietal cortex in freely moving mice. We found that theta phase dynamically modulates distinct gamma bands during REM sleep. Interestingly, we further show that theta–gamma coupling switches between recorded brain structures during REM sleep and progressively increases over a single REM sleep episode. Finally, we show that optogenetic silencing of septohippocampal GABAergic projections significantly impedes both theta–gamma coupling and theta phase coherence. Collectively, our study shows that phase-space (i.e. cross-frequency coupling) coding of information during REM sleep is orchestrated across time and space consistent with region-specific processing of information during REM sleep including learning and memory.

Significance

Classical descriptions of sleep-related brain activity using low spatial resolution electroencephalography led to the distinction between non-rapid eye movement (NREM) and REM (or paradoxical) sleep. Yet, local brain activity during each of these states is characterized by circuit-specific oscillations (slow waves, spindles, and theta). In this study, we show that theta–gamma cross-frequency coupling (CFC) in the hippocampus is dynamically modulated in space and time during single REM sleep episode, distinct from neocortical CFC. These findings extend the multiple criteria used to define REM sleep state in health and disease.

Key words: REM sleep; active wake; theta–gamma coupling; optogenetics; hippocampus

Introduction

Both rapid eye movement (REM) and non-REM (NREM) sleep are associated with consolidation of some aspects of memory following task acquisition in rodents and humans [1–7]. Classically, the reactivation of hippocampal place cells during NREM sleep provides one possible mechanism for the long-term encoding of newly acquired spatial [1, 8] but also procedural and emotional information [9–11]. However, the underlying mechanisms of memory consolidation during REM sleep are unclear. Recent work involving in-depth analysis of local field potentials (LFPs) recorded from memory-associated brain structures, which includes the hippocampus or neocortex, has provided a possible neural mechanism for memory consolidation [12–14]. One of these includes phase-amplitude cross-frequency coupling (CFC), a phenomenon that describes the increased modulation of fast oscillation amplitude by slow oscillation phase during cognitive and perceptual tasks [15–18]. Specifically, hippocampal and cortical phase-amplitude theta–gamma coupling is prevalent during locomotion and REM sleep in rodents [19, 20] and increases during behavioral and learning tasks in rodents [21, 22], monkeys [23, 24], and humans [25–27]. In addition, dynamic phase entrainment of low-frequency oscillations (<15 Hz) during cognitive tasks and sensory inputs has also been described [28, 29]. Furthermore, impaired phase–amplitude coupling has been reported in Alzheimer's disease [30, 31], schizophrenia [32], and Parkinson's disease [33]. Thus, the existence of phase–amplitude coupling and phase entrainment of low frequencies suggests a broad implication of CFC of network oscillations in hierarchical information processing essential to cognitive functions during wakefulness or sleep (for a review see [34]).

The hippocampal formation is essential for the learning and storage of information related to fundamental behaviors [35]. Theta and gamma are predominant oscillations during active wake and REM sleep in rodent hippocampal structures and are increased by spatial navigation and learning tasks [36]. Theta rhythm in the hippocampus is generated through extrinsic [3, 37] and intrinsic mechanisms [38, 39]. We recently showed that hippocampal theta rhythm during REM sleep is essential to contextual memory consolidation [3]. Indeed, optogenetic silencing of medial septal GABAergic (MS^{GABA}) neurons during REM sleep (extrinsic inputs) impaired contextual memory of a previously acquired fear-conditioned task in mice.

Here, we characterize the phase–amplitude coupling between theta and fast oscillations in hippocampal LFP and cortical electrocorticographic (ECoG) recordings of freely moving mice during spontaneous sleep–wake states and upon optogenetic perturbation of MS^{GABA} neurons during REM sleep. We found that episodes of both active wake and REM sleep showed significant theta–middle gamma coupling, with the highest level of coupling observed during REM sleep. Theta–high gamma coupling was also present during REM sleep, but not during active wake. We further found that theta–gamma coupling is a discrete phenomenon that switches between hippocampal and cortical structures and increases over a single REM sleep episode. Finally, we extended our analysis to previously acquired optogenetic dataset and found that optogenetic silencing of MS^{GABA} neurons impeded phase–amplitude coupling and theta phase coherence in the hippocampus and neocortex during REM sleep.

Materials and Methods

Animals

We used male VGAT-ires-Cre (VGAT::Cre) transgenic mice (Jackson Laboratory). All mice were housed individually in polycarbonate cages at constant temperature (22 ± 1°C), humidity (30%–50%), and light cycle (12 h:12 h, light:dark; lights on at 0800). Mice were allowed unlimited access to food and water. Animals were treated according to protocols and guidelines approved by McGill University and the Canadian Council of Animal Care. Data included in this study were collected from new experimental procedures or a prior study (Figure 2 and Supplementary Figure 4) [3].

Virus-mediated targeting of opsin and eYFP expression

For optogenetics experiments, transgenic mice were anesthetized with isoflurane (5% induction, 1%–2% maintenance) and placed in a stereotaxic frame at approximately 10 weeks age. Recombinant AAVdj-EF1alpha-DIO-ArchT-eYFP virus (eYFP = enhanced yellow fluorescent protein) (0.6 μL) was stereotactically injected into the medial septum (relative to bregma, in mm; Anterior–Posterior [AP]: +0.86; Medial–Lateral [ML]: 0.0; Dorsal-Ventral [DV] –4.5) of anesthetized mice. An in-depth evaluation of the precision and efficacy of the genetic targeting strategy and ArchT-expression silencing of MS^{GABA} neurons was reported in a prior study [3].

Electrode and optic fiber implantation

Tetrodes were made by twisting four individual 17.5 μm diameter platinum–iridium (platinum:iridium 90%:10%) wires into a single strand. For targeting dorsal hippocampal CA3, CA1, and subiculum, leads from 3 tetrodes were then soldered to an electrode interface board and fixed in the correct orientation using epoxy to facilitate implantation as a single array. Tetrode ends were cut to the appropriate length in relation to one another and subsequently cleaned immediately before surgery, giving a measured impedance of approximately 1 MΩ. At 18 weeks age, mice were anesthetized with isoflurane (5% induction, 0.5%–2% maintenance) and subsequently placed in a stereotaxic frame. After clearing the skull of connective tissue and drying with alcohol, holes were drilled in the bone above the dorsal hippocampus (relative to bregma, in mm; CA3: AP: –1.8, ML: +2.1; CA1: AP: –2.45, ML: +1.8; subiculum: AP: –3.10, ML +1.5). The dura was gently cut, and the electrode array was slowly lowered until the tips of the tetrodes in the prearranged array were at the correct depth (CA3: DV: –2.25; CA1: DV: –1.3; subiculum: DV: –1.5; Supplementary Figure 1). A similar procedure was used for implantation of silicon probes (NeuroNexus) used to record laminar LFPs at 50 μm increments oriented vertically through hippocampal CA1, although slightly different coordinates were used for optimal orientation of the probe perpendicular to the CA1 layers (AP: –2.45, ML: +1.5, probe tip DV: –1.5). In all experiments, a screw implanted in the skull above the parietal cortex (AP: –2.3; ML: –1.35), which contacted the surface of brain tissue and served as ECoG, and two stranded tungsten wires inserted into the neck musculature used as EMG signals for assessing postural tone. Screws placed in the bone above the frontal cortex and cerebellum served as ground and reference, respectively. For

optogenetics experiments, an optic fiber implant that used to deliver laser light to the MS virus-transfection zone was implanted just above the MS (AP: +0.86; ML: −0.2; DV: −3.82; Supplementary Figure 1). As a final step, dental cement was applied to the skull to permanently secure all components of the implant.

In vivo electrophysiological recording

Mice were allowed to recover from surgery for at least 1 week. Afterward, a headstage preamplifier tether was attached to a connector on the top of the implanted electrode interface board. Mice were subsequently returned to their home cage where they were allowed to habituate to the tether system for 1 week. Once mice were habituated to the chronic tethering system, a consecutive 24-h recording was completed for all mice. For optogenetics experiments, a 2-h recording session was conducted to assess how disrupting MS^{GABA} activity would influence CFC and theta phase coherence during REM sleep. Mice were continuously monitored until they entered into at least 10 s of stable REM sleep (see criteria in "Determination of vigilance states"). Continuous square pulses of orange light, approximately 7 s in duration, were delivered to the MS area via the optic fiber implant at a frequency of approximately 2 pulses/min. This protocol was continued until mice transitioned to wakefulness, at which point MS^{GABA} silencing ceased until subsequent REM sleep occurred. The intensity of light delivered to the MS was calibrated to approximately 20 mW, a value that, in the absence of ArchT expression, was previously shown to have no effect on baseline electroencephalogram (EEG) characteristics and animal behavior [3]. The precise onset and offset of light delivery were timestamped to neurophysiological recordings. For each session, all recorded signals from the implanted electrodes were amplified by the headstage preamplifier tether before being digitized and acquired at 16 kHz sampling rate using a digital recording system (Neuralynx). To obtain LFP/ECoG/EMG signals, we downsampled raw traces into 1,000 Hz using the "decimate" function of MATLAB, which applies a low pass filter (400 Hz, 8th order Chebyshev Type I) before downsampling to prevent aliasing and spike contamination.

Histological confirmation

After completion of experiments, mice were deeply anesthetized by intraperitoneal injection of ketamine/xylazine/acepromazide (100, 16, and 3 mg/kg, respectively) and electrode sites were subsequently marked by passing a 10 µA current for approximately 10 s through each tetrode. After lesioning, mice were perfused transcardially with 1× PBS-heparin 0.1%, pH 7.4, followed by 4% paraformaldehyde (PFA) in phosphate-buffered saline (PBS). Brains were removed from the skull and placed in PFA at 4°C overnight before being cryoprotected in 30% sucrose dissolved in PBS at 4°C for an additional 24 h. Brains were then sectioned (50 µm) using a cryostat; half of sections collected were further processed to evaluate accuracy of ArchT-eYFP construct expression, whereas the remaining sections were mounted on gelatin-coated glass slides, stained with cresyl violet, and coverslipped. Final electrode and optic fiber locations were determined by viewing these stained sections with a light microscope. Only mice with confirmed placement of electrodes in the CA3 pyramidal layer, CA1 stratum radiatum (all layers for silicon probe-implanted mice), and the subiculum pyramidal layer, as well as proper optic fiber tip placement immediately above the MS transfection zone for optogenetics experiments, were further analyzed.

To confirm accurate targeting of the ArchT-eYFP construct to MS^{GABA}, sections not used for electrode/fiber localization were initially washed in PBS 1×-Triton (0.3%) (PBST) and then incubated for 60 min at room temperature in a blocking solution, composed of 4% bovine serum albumin (BSA) dissolved in PBST, before being incubated in rabbit anti-green fluorescent protein (GFP) (diluted 1:5000 in BSA) overnight at 4°C. To detect the primary antibody, sections were incubated the following day in Alexa Fluor 488 ex anti-rabbit IgG (H + L) (diluted 1:1,000 in PBST) for 1 h at room temperature, before being mounted onto glass slides and coverslipped with Fluoromount-G. Once slides were sufficiently dry, fluorescent images of immunolabelled sections were acquired using a fluorescent microscope. Only mice with confirmed construct expression restricted to neurons localized within the MS and diagonal band regions were further analyzed.

Determination of vigilance states

Vigilance state was manually scored in 5-s epochs for all recordings through the concurrent evaluation of ECoG signals, EMG-derived muscle activity, and video monitoring of behavior. Quiet wake was defined as awake periods in which mice were immobile with the absence of theta band ECoG activity and tonic muscle activity. Active wake was defined as periods of theta band ECoG activity and EMG bursts of movement-related activity. NREM sleep was identified as periods with a relative high-amplitude, low-frequency EcoG, and reduced muscle tone relative to quiet wake. REM sleep was defined as sustained periods of theta band ECoG activity and behavioral quiescence associated with muscle atonia, save for brief phasic muscle twitches. To avoid mixed states (or transitions), we excluded the ± 5 s epochs during transition periods from our analysis. Polysomnographic scorings were performed double-blinded and were statistically confirmed to lie within a 95% confidence interval (Supplementary Figure 2) [40].

Data analysis

All simulations and analyses were performed in MATLAB (R2016a, Natick, MA) environment using custom scripts and built-in functions available on request.

Modulation Index

We used the Modulation Index (MI) to measure phase–amplitude coupling [22]. We first bandpass-filtered LFP/ECoG signals into low- and high-frequency bands, i.e. theta (6–10 Hz) and middle gamma (50–90 Hz), using finite impulse response (FIR) filters in both forward and reverse directions to eliminate phase distortion ("filtfilt" function, MATLAB). We designed FIR filters using the window-based approach ("fir1" function, MATLAB) with an order equal to three cycles of the low cutoff frequency. We then estimated instantaneous phase of low frequency and the envelope of high frequency oscillations using the Hilbert transform. Then, phase of the low frequency was discretized into 18 equal bins ($N = 18$, each 20°) and the average value of fast oscillations' envelope inside each bin was calculated. The

resulting phase-amplitude histogram (*P*) was compared with a uniform distribution (*U*) using the Kullback–Leibler distance, $D_{KL}(P,U) = \sum_{j=1}^{N} P(j) * log[P(j)/U(j)]$, which was normalized by *log(N)* to obtain MI, $MI = D_{KL}/log(N)$.

Comodulogram analysis

MI-based comodulogram analysis is a powerful tool to assess phase–amplitude coupling for a wide range of frequencies, as MI is independent of power of fast frequencies and comodulogram graph is not biased for bands with a higher power. To explore coupling between different pairs of frequency bands, we considered 18 frequency bands for phase (0.5–18.5 Hz, 1-Hz increments, 2-Hz bandwidth), and 28 frequency bands for amplitude (20–310 Hz, 10-Hz increments, 20-Hz bandwidth). MI values were then calculated for all these pairs to obtain the comodulogram graph. For each animal, we first filtered continuous 24-h recordings into the mentioned frequency bands and estimated the Hilbert transform. Then, we concatenated episodes of each vigilance state to derive the stage-specific comodulogram graphs. To avoid power line interferences, frequency bands in the vicinity of 60 Hz and its harmonics were reassigned with a 2-Hz safe margin from these interfering frequencies.

Time-resolved phase–amplitude coupling

We used a time-resolved approach to track changes of phase–amplitude coupling in both time and frequency domains [41]. We first bandpass-filtered the LFP/ECoG signal into 24 sub-bands for amplitude frequency, as described in "Comodulogram Analysis" section, and obtained envelopes of filtered signals using the Hilbert transform. We segmented the resulting envelopes into 4-s windows having 75% overlap and calculated the fast Fourier transform (FFT) for each segment. To minimize the side effects of filtering on signal edges, we applied segmentation after filtering. The frequency band for the phase was obtained from the envelope of the filtered signal for the amplitude frequency band. We estimated the peak frequency of the envelope using the FFT, and then bandpass-filtered LFP/ECoG signals at this peak frequency using a 2-Hz bandwidth. MI was then calculated between the phase of this frequency band and the corresponding high-frequency band. The logic behind this approach is that if there is phase–amplitude coupling between low and high-frequency bands, the modulating low frequency and dominant frequency of envelope of the modulated fast frequency are similar. Therefore, we can track coupling dynamics over time and frequency by replacing phase-frequency axis in the comodulogram (horizontal axis) with the time axis.

Theta phase coherence

We estimated the phase coherence in the theta range between two signals using mean phase coherence [42], which is the most prominent measure of phase synchronization. To obtain theta phase coherence, we first filtered LFP/ECoG traces in the theta range (6–10 Hz) using a 500th-order FIR filter ("fir1" function, MATLAB) in both the forward and reverse directions. Afterward, we extracted the instantaneous phases of filtered signals using the Hilbert transform and obtained theta phase coherence by

averaging the instantaneous phase differences of two filtered signals projected onto a unit circle in the complex plane. This measure has a value between [0 1], where zero and one indicate completely incoherent and coherent theta rhythms, respectively.

Spectral analysis

We estimated power spectral density (PSD) using Welch's method ("pwelch" function, MATLAB) with 4-s segments having 75% overlap. Simply, the Welch's method applies a Hamming window on each segment, calculates the FFT of segments, and then averages over all resulting FFTs. We obtained time–frequency representations using the multitaper method from Chronux signal processing toolbox (window size = 3 s, step size = 0.1 s, tapers [3 5]).

Statistical analysis

The reported values are mean with the standard error of the mean (mean ± SEM). Two-tailed Wilcoxon signed-rank test and two-way repeated-measures ANOVA were used for the reported statistics, unless otherwise mentioned. To evaluate phase–amplitude coupling results, surrogate data test was performed to test significance for MI values. Surrogate data were generated by shuffling the phase of low-frequency bands 200 times, and MI values were calculated between these shuffled phase time series and the envelope of the amplitude frequency. Reported *P* values were calculated by dividing the number of surrogate MI values greater than the original MI value by 200.

Results

LFPs were simultaneously recorded in the hippocampal pyramidal layers of CA3 and subiculum, hippocampal CA1 stratum radiatum, as well as ECoG in the parietal cortex (PCx) across vigilance states in freely moving mice (Figure 1A). We calculated phase–amplitude coupling using the MI [22] and assessed this CFC for a wide range of slow and fast oscillations using the comodulogram analysis. To investigate dynamics of coupling across multiple frequency and temporal scales, we computed the MI using the time-resolved approach.

Theta modulates distinct gamma bands during REM sleep

To assess general patterns of phase–amplitude coupling during vigilance states for each recorded site, we calculated state-specific comodulograms for active wake, REM sleep, and NREM sleep from continuous 24-h recordings (Figure 1A and B and Supplementary Figure 3). We found that theta phase (6–10 Hz) significantly modulates amplitude of middle gamma band (gamma$_M$: 50–90 Hz) during active wake and REM sleep within the CA3, CA1, subiculum, and PCx recordings (*P* < 0.001 for all sites, surrogate test; Figure 1B and C). Theta–gamma$_M$ coupling significantly increased for subiculum and PCx, but not for CA3 and CA1, recordings during REM sleep compared to active wake (REM sleep vs. active wake: *P* < 0.001; *n* = 7 animals; two-way ANOVA; Figure 1D and Supplementary Table 1). During REM sleep, in addition to theta–gamma$_M$ coupling, theta
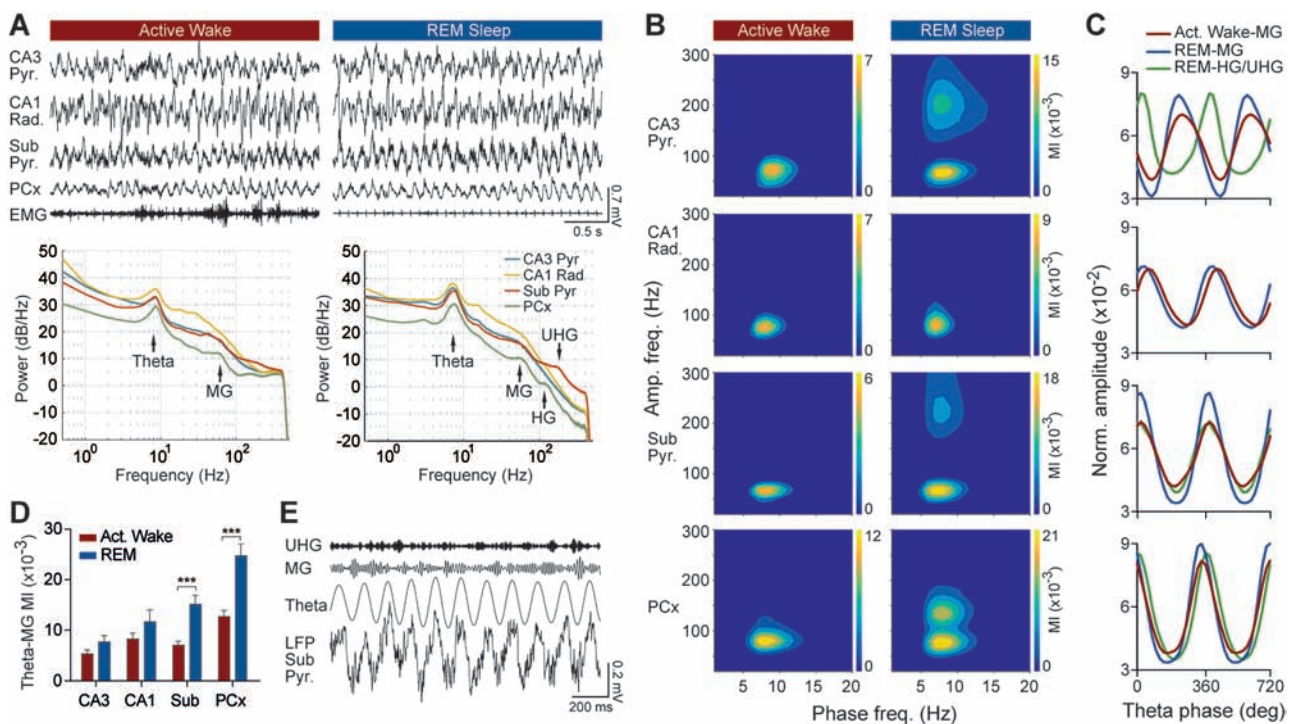
Figure 1. General patterns of phase-amplitude coupling during active wake and REM sleep. (A) Representative recordings from pyramidal layers of CA3 and subiculum, CA1 radiatum, PCx, and EMG signal during active wake and REM sleep. Power spectral densities obtained from 24-h recordings. Note the distinguishable peaks within fast oscillations during REM sleep. (B) Comodulogram graphs show MI for a wide range of frequency pairs, obtained from 24-h recordings of one animal. (C) Corresponding phase–amplitude histograms for theta–gamma$_M$ and either theta–gamma$_H$ or theta–gamma$_{UH}$ coupling during active wake and REM sleep for the same animal as in panel (B). The distributions are consistent across animals. Zero and 180 degrees correspond to trough and peak of local theta cycle, respectively. (D) Quantification of theta–gamma$_M$ coupling during active wake and REM sleep (REM sleep vs. active wake: $P < 0.001$; $n = 7$ animals; two-way ANOVA). Coupling during REM sleep is significantly stronger than active wake within the subiculum and PCx, but not within CA3 and CA1. (E) Example of gamma$_{UH}$ in the pyramidal layer of subiculum during REM sleep.

phase significantly modulated high gamma (gamma$_H$: 110–160 Hz) in the PCx ($P < 0.001$, surrogate test), and the ultrahigh gamma (gamma$_{UH}$: 160–250 Hz) in pyramidal layers of CA3 and subiculum ($P < 0.001$ for both, surrogate test; Figure 1B–E). Theta–gamma$_M$ coupling was stronger than theta–gamma$_H$ and theta–gamma$_{UH}$ coupling during REM sleep for all sites (Figure 1B). During NREM sleep, ripples (150–250 Hz) that are generated from synchronous bursts of neural activity in the hippocampal formation, exhibited coupling to sharp waves within the CA3 pyramidal layer and CA1 stratum radiatum (Supplementary Figure 3). Note that NREM ripples of subicular pyramidal layer were phase-coupled to both slow waves (0.5–1.5 Hz) and spindles (Supplementary Figure 3B).

To find the preferred theta phases for gamma during active wake and REM sleep, we used phase-amplitude histograms obtained for calculation of the MI. We analyzed CA3, subiculum and PCx recordings that showed distinct coupling patterns both in gamma$_M$ and either gamma$_H$ or gamma$_{UH}$ during REM sleep (Figure 1C). We found that the gamma$_{UH}$ modulation phase lagged behind gamma$_M$ modulation by approximately 90° (~32 ms time delay) in CA3 pyramidal layer, whereas no difference was observed for the subicular pyramidal layer during REM sleep. For the PCx, a slight difference of approximately 20° (~8 ms time delay) was found between preferential theta phases of gamma$_M$ and gamma$_H$. Furthermore, comparing preferred theta phase for gamma$_M$ during active wake and REM sleep revealed no significant difference (Figure 1C). Collectively, these results showed a state- and region-specific

phase–amplitude coupling in the hippocampus and neocortex of mice.

Optogenetic silencing of MS^{GABA} neurons suppresses theta–gamma coupling and theta phase coherence

We previously showed that optogenetic silencing of MS^{GABA} neurons during REM sleep impairs both object recognition and fear-conditioned contextual memory in mice [3]. To investigate possible underlying mechanisms, we computed theta–gamma coupling, theta phase coherence, and PSD of recordings before, during, and after silencing of MS^{GABA} neurons during REM sleep (Figure 2A and approximately Table 2) from animals recorded in a previous study [3]. We found that optogenetic silencing of MS^{GABA} neurons significantly decreases theta–gamma coupling during REM sleep (silencing vs. baseline; $P < 0.001$ for all sites and gamma bands; $n = 4$ animals, 10 silencing trials each; one-way ANOVA with multiple comparison tests; Figure 2B). Furthermore, there was a strong phase coherence in the theta range between recorded sites before and after optogenetic silencing, while significantly decreased during MS^{GABA} silencing (silencing vs. baseline; $P < 0.001$ for all pairs; $n = 4$ animals; 10 trials each; Figure 2). Consistent with the previous study [3], we also found that although theta power was significantly reduced during silencing, gamma power showed no significant changes (theta: $P < 0.001$ for all sites; gamma: $P > 0.05$ for all sites and gamma bands; $n = 4$ animals, 10 trials each; one-way ANOVA with multiple comparison tests; Figure 2A and F).
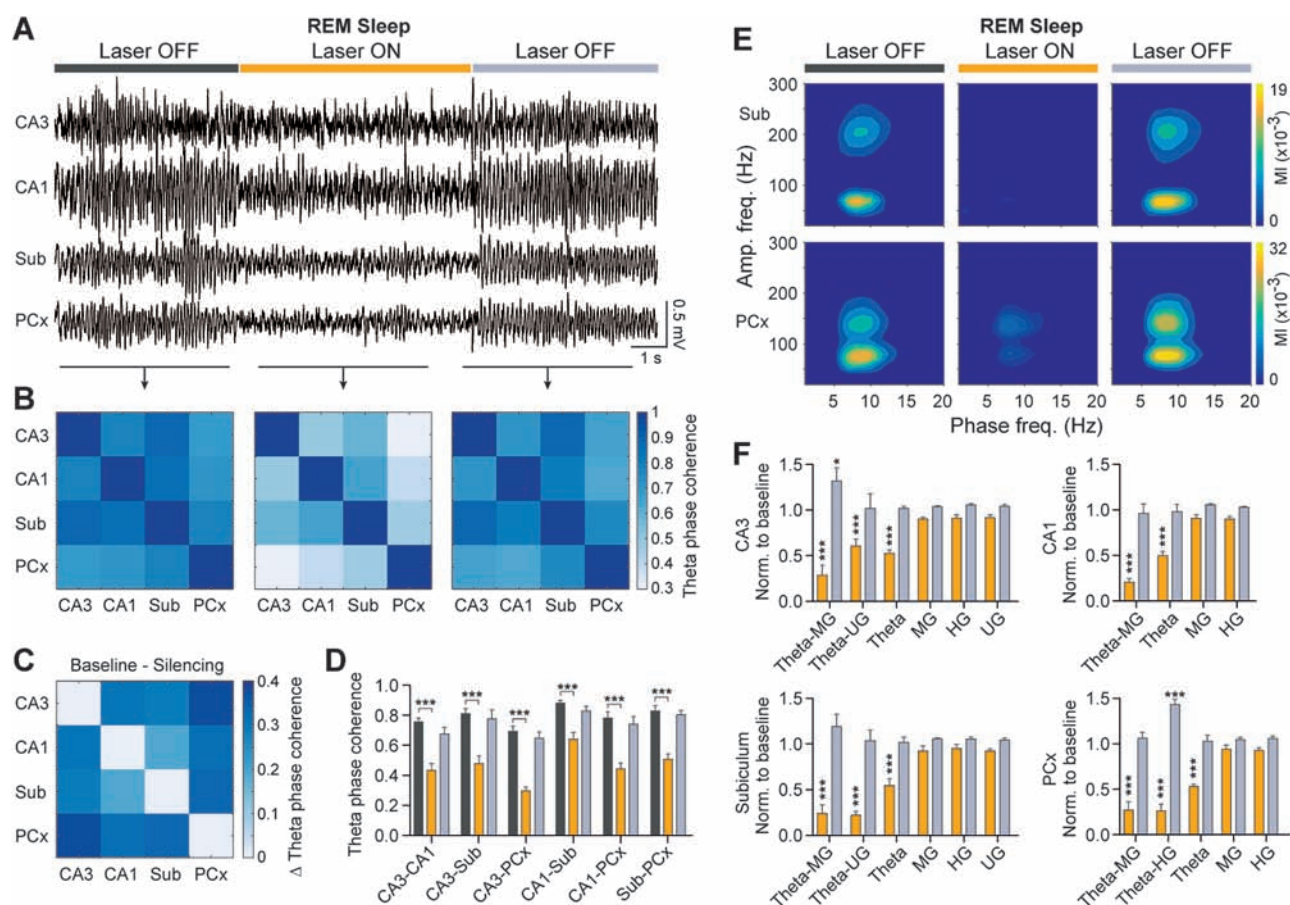
Figure 2. Optogenetic silencing of extrinsic theta projections disrupts theta–gamma coupling and theta phase coherence. (A) Representative recordings before, during, and after silencing of MS^{GABA} neurons during REM sleep. Baseline was considered as 5 s of REM sleep immediately before silencing. (B) Theta phase coherence between CA3, CA1, subiculum, and PCx sites during baseline, silencing, and post silencing. Graphs show average results from four animals, 10 silencing trials each. (C) Difference in theta phase coherence between baseline and silencing. The highest decrease in phase coherence was between CA3 and PCx sites, which dropped from approximately 0.7 to approximately 0.3. (D) Quantification of theta phase coherence. There is a strong theta phase coherence between recorded sites before and after silencing, whereas coherence significantly decreased during MS^{GABA} silencing (silencing vs. baseline; $P < 0.001$ for all pairs; $n = 4$ animals, 10 trials each). (E) Comodulogram graphs before, during and after MS^{GABA} silencing estimated from 10 trials of one animal. (F) Quantification of theta–gamma coupling and theta/gamma power during and after silencing compared to the baseline (silencing vs. baseline; $P < 0.001$ for all sites and gamma bands; $n = 4$ animals, 10 silencing trials each; one-way ANOVA with multiple comparison tests). Vertical and horizontal asterisks are same.

Dynamic modulation of theta–gamma coupling during REM sleep

To investigate dynamics of the phase–amplitude coupling during REM sleep, we used a time-resolved approach (Figure 3A). We found that theta–gamma coupling "waxes and wanes" over time during a single REM sleep episode that corresponds to a discrete and transient phenomenon lasting for only few seconds with no detectable periodicity. We also used the time-resolved phase-locking value (PLV) as a control measure of phase–amplitude coupling (Figure 3B). Interestingly, this dynamic regulation of CFC is independent of the existence of gamma activity over the whole course of a REM sleep episode (Figure 3C). Figure 3D shows the dominant frequency of fast oscillation envelope, which was used as phase frequency to obtain time-resolved MI and PLV measures in Figure 3A and B.

To assess the dependency of theta–gamma coupling strength on theta and gamma power, we calculated the normalized cross-correlation between theta–gamma$_{M}$ coupling and theta/gamma power time series, which were estimated using a 4-s moving window with 75% overlap (Figure 3E and F; Supplementary Figure 5 and Table 3). We found that the

normalized cross-correlation between theta–gamma$_{M}$ coupling and theta/gamma power time series is very weak (CA3: MI-theta: 0.19 ± 0.03, MI-gamma: 0.18 ± 0.05; Supplementary Table 3), indicating that an increase in coupling is not a reflection of a higher theta and/or gamma power. We further quantified the normalized cross-correlation between theta power and gamma power (Figure 3G), and we found that their power is independent of each other (CA3: theta–gamma: 0.06 ± 0.03; Supplementary Table 3). These results show that phase–amplitude coupling in hippocampo-cortical structures is dynamically regulated over time, as evidence for other network oscillations, e.g. thalamocortical spindles, during sleep [36, 43].

Theta–gamma coupling is spatially orchestrated during REM sleep

The discrete nature of theta–gamma coupling raises the question as to whether CFC is locally modulated. To assess this, we studied dynamics of theta–gamma$_{M}$ coupling from simultaneous LFPs recordings from electrodes located in CA3, CA1, subiculum, and PCx during active wake and REM
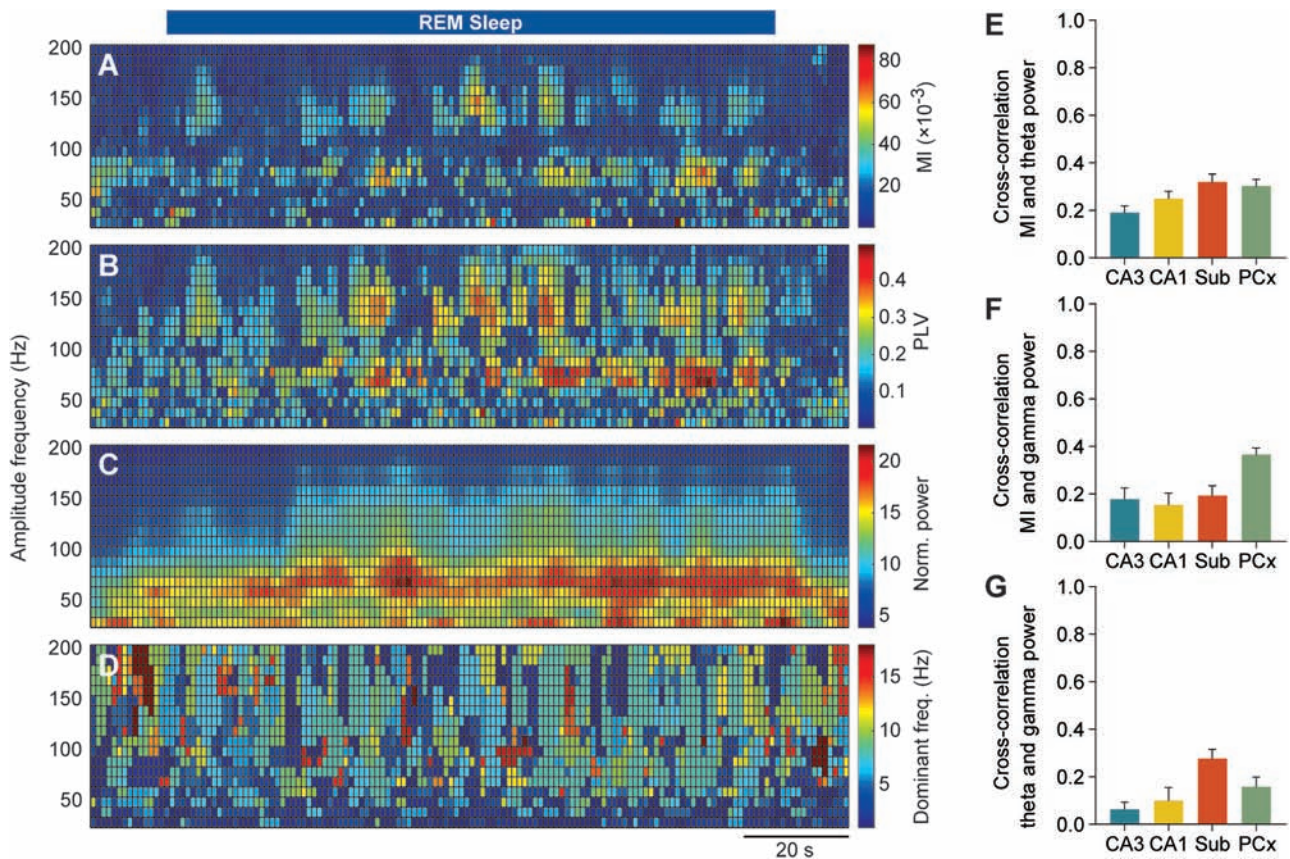
Figure 3. Dynamics of phase–amplitude coupling during REM sleep. (A, B) Time-resolved MI and PLV measures estimated from PCx across a REM sleep episode. Horizontal and vertical axes are time and modulated frequencies (i.e. gamma range), respectively. Blue horizontal line in the top of graphs indicates REM sleep. (C) Normalized power of fast oscillations during REM sleep. Power of amplitude-frequency bands was normalized to their first 10 s average power to provide meaningful comparison between frequency bands. (D) Dominant frequency of the envelope of fast oscillations, which is considered as phase frequency or modulating frequency, in the time-resolved approach. All measures were estimated using a moving window of 4 s having 75% overlap during a REM sleep episode. (E, F) Normalized cross-correlation between theta–gamma$_M$ coupling and theta/gamma power time series, which were estimated using a 4-s moving window with 75% overlap for all the recording sites. (G) Same as panel (E), except for theta and gamma power. The normalized cross-correlation between theta–gamma$_M$ coupling and theta/gamma power time series, as well as between theta and gamma power time series are very weak (n = 7 animals).

sleep. Interestingly, we found that theta–gamma$_M$ coupling switches between recorded sites, while it coexists during short periods of time in pairs of recordings (Figure 4A). Importantly, theta–gamma$_M$ coupling switches did not occur in between CA1 layers as assessed by linear silicon probe recordings (Figure 4B), suggesting uniform modulatory input. To quantify concurrent coupling between hippocampal and neocortical recording sites, we estimated the overlap ratio and cross-correlation between pairs of channels during active wake and REM sleep (Figure 4C and D). Overlap ratio was restricted to periods where at least one region showed high levels of theta–gamma$_M$ coupling (1.5 SD + mean) and indicates portion of these times that two sites exhibited theta–gamma$_M$ coupling higher than 1.5 SD above the mean, simultaneously. We found that overlap ratio significantly increased during REM sleep compared to active wake for all the studied pairs, except for CA3-PCx (REM sleep vs. active wake: P = 0.002; n = 7 animals; two-way repeated-measures ANOVA; Figure 4C and Supplementary Table 4). Cross-correlation value was obtained considering whole periods during active wake or REM sleep and increased significantly during REM sleep

compared to active wake for all the recording pairs (REM sleep vs. active wake: P < 0.001; n = 4 animals; two-way repeated-measures ANOVA; Figure 4D and Supplementary Table 4).

To examine the existence of periodicity in coupling, we measured distance between theta–gamma$_M$ coupling events (intercoupling interval) within individual active wake and REM episodes. We found that intercoupling interval varies from few seconds to tens of seconds (ECoG: 16.9 ± 0.4 s); however, the average and distribution of intercoupling interval is quite consistent across active wake and REM sleep (Figure 4E; Supplementary Figure 6 and Table 1). To assess the correlation between eye movements and theta–gamma coupling during REM sleep, we recorded simultaneous EEG, EMG, and electrooculogram signals from 4 mice. We estimated the theta–gamma coupling during REM sleep periods with and without eye movement activity, but no significant difference was found between the coupling values of two groups (Supplementary Figure 7). Thus, our results suggest a region-specific modulation of theta–gamma coupling during REM sleep that may support information transfer during sleep-dependent consolidation of information storage [44].
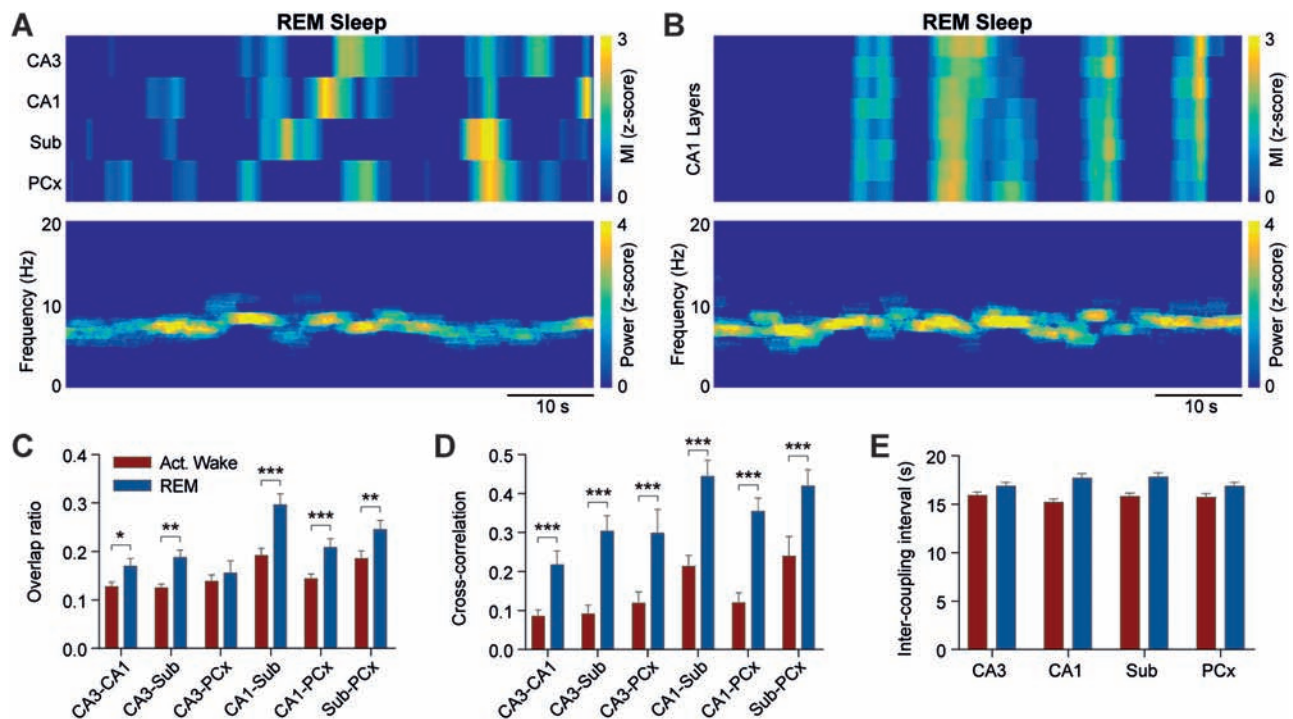
Figure 4. Theta–gamma coupling swings between hippocampal and cortical circuitries during REM sleep. (A) Top graph shows dynamics of theta-gamma$_M$ coupling over a REM sleep episode for CA3, CA1, subiculum, and PCx recordings. Coupling mainly switches between networks, but co-occurs during short periods of time. The MI measure was estimated using a moving window of 4 s having 75% overlap, and then smoothed by a 10-point Hanning window. Bottom graph illustrates corresponding time-frequency representation. (B) Same as panel (A), except for different layers of CA1. Theta–gamma$_M$ coupling is highly synchronized across the layers of CA1. (C) Quantification of coupling concurrency between recording pairs during active wake and REM sleep. Overlap ratio indicates the proportion of times that two regions simultaneously show theta–gamma$_M$ coupling higher than 1.5 SD above the mean. Overlap ratio significantly increased during REM sleep compared to active wake for all the studied pairs, except for CA3-PCx (REM sleep vs. active wake: $P = 0.002$; $n = 7$ animals; two-way repeated measures ANOVA). (D) Normalized cross-correlation between theta–gamma$_M$ coupling time series of different recording pairs that is obtained considering whole periods during active wake or REM sleep. Normalized cross-correlation increased significantly during REM sleep compared to active wake for all the recording pairs (REM sleep vs. active wake: $P < 0.001$; $n = 4$ animals; two-way repeated measures ANOVA). (E) Average distance between theta–gamma$_M$ coupling episodes. Intercoupling interval indicates silent periods between two coupling events. The average intercoupling interval is quite consistent across active wake and REM sleep.

Theta–gamma coupling is strengthened during a single REM episode

Temporal representations of theta–gamma coupling during individual REM sleep episodes suggested that it progressively increases over time within a single episode of REM sleep (Figure 3A and Figure 4A). To further verify this, we divided each REM episode into three equal "early/middle/late" segments and calculated theta–gamma$_M$ coupling and theta/gamma$_M$ power for each segment and normalized middle and late values to the early segment. We included only REM episodes lasting more than 30 s for this analysis to provide segments with at least 10 s length. We found that the theta–gamma$_M$ coupling significantly increased across REM sleep for all recorded sites (late vs. early REM segment: $P < 0.001$ for all sites; $n = 7$ animals; Wilcoxon test; Figure 5A; Supplementary Table 5). No significant change in theta power across REM sleep was observed (late vs. early REM segment: $P > 0.05$ for all sites except Sub; $n = 7$ animals; Wilcoxon test; Figure 5B), whereas gamma$_M$ power significantly increased (late vs. early REM segment: $P < 0.001$ for all sites; $n = 7$ animals; Wilcoxon test; Figure 5C). We did not find any linear correlation between duration of REM episode and variations in MI. However, shorter REM episodes showed less variations in coupling across episodes (Figure 5D). In CA3 and CA1, average relative MI showed the highest increase for REM episodes with approximately 70 s

duration, with decreasing values for longer REM sleep episodes in CA3, whereas remained almost stable in CA1 after approximately 70 s. The MI variations in the subiculum and PCx were less dependent on duration of REM sleep, consistent with the overall modulation of theta–gamma coupling in both space and time.

Discussion

Our findings show that theta–gamma coupling in the hippocampus and neocortex is dynamically modulated in time and space during REM sleep. Importantly, our results emphasize that this modulation strongly fluctuates within a single REM sleep episode, a previously unappreciated feature of the neural circuits' activity during this sleep state. Although the mechanism underlying this dynamic modulation of brain activity during REM sleep remains unknown, this modulation likely reflects local coordination of their inputs/outputs at a given time that supports communication between regional networks while minimizing interference [45]. Indeed, coupling predominantly switches between CA3, CA1, subiculum, and PCx networks, although they co-occur in these structures for relatively short periods of time. The overlap ratio and cross-correlation analysis between theta–gamma$_M$ coupling events of LFPs recorded from pairs of
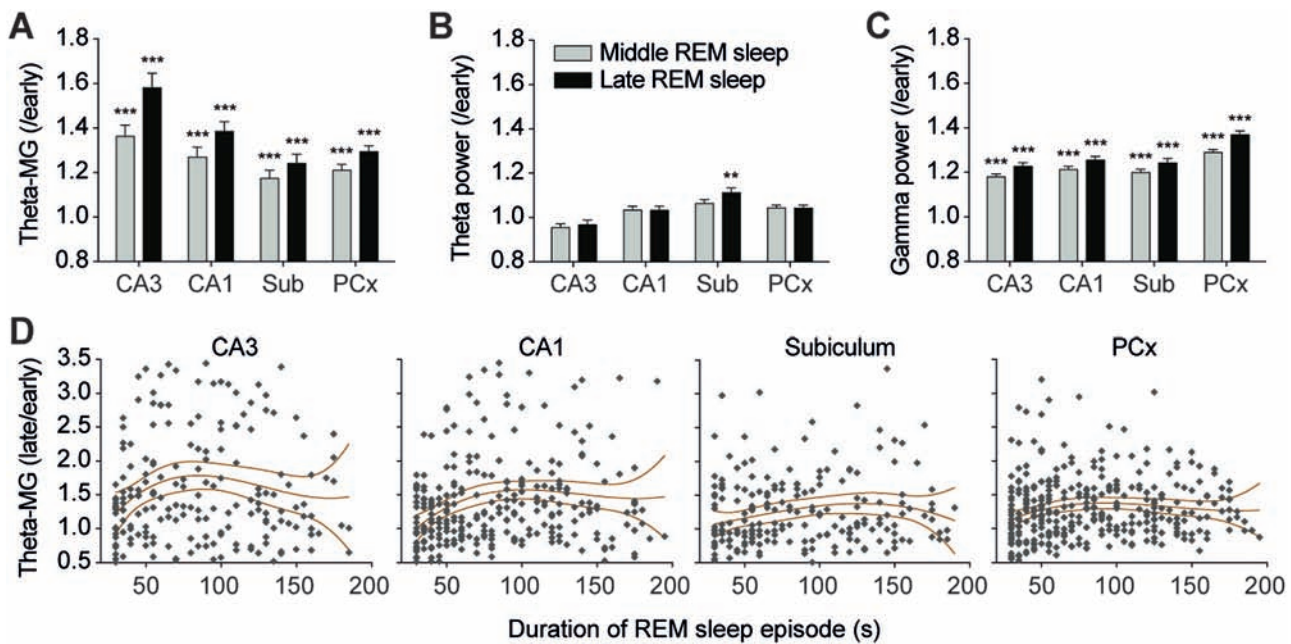
Figure 5. Theta–gamma coupling strength increases over REM sleep episodes. (A) Normalized theta–gamma$_M$ coupling during middle and late phases of REM sleep episodes for CA3, CA1, subiculum, and PCx recordings. For each REM episode, middle and late coupling values were normalized to the early segment. Theta–gamma$_M$ coupling significantly increased for all sites (late vs. early REM segment: $P < 0.001$ for all sites; $n = 7$ animals; Wilcoxon test). (B, C) Same graphs as panel (A) but for theta and gamma$_M$ power, respectively. Theta power showed no significant changes across REM sleep, except within the subiculum, whereas gamma$_M$ power significantly increased (late vs. early REM segment: theta: $P > 0.05$; gamma$_M$: $P < 0.001$ for all sites; $n = 7$ animals; Wilcoxon test). (D) Relation between duration of REM episodes and variations in theta–gamma$_M$ coupling. Each point represents one REM sleep episode and lines indicate mean ± SEM of points.

electrodes exhibited greater synchronized coupling during REM sleep compared to active wake for all pairs (Figure 4C and D). Furthermore, the intercoupling interval histograms had similar distributions for active wake and REM sleep (Supplementary Figure 6), indicating that the increase in concurrent coupling between brain structures during REM sleep, compared to active wake, is due to the way in which theta–gamma$_M$ coupling is orchestrated, and not simply the result of increased number of coupling events. These observations can be interpreted as a co-activation of two, or more, circuits during REM sleep, which may provide windows of consolidation of previously acquired information.

The increase of theta–gamma$_M$ coupling in subicular and cortical, but not CA3 and CA1, structures during REM sleep compared to active wakefulness may reflect a possible role for subiculum and cortex as anatomical and functional outputs in the hippocampal–neocortical dialog supporting long-term memory [44]. One can speculate that considering phase–amplitude coupling as a mechanism for the processing and transmission of information [31, 45, 46], low level of theta–gamma$_{UH}$ coupling during active wake may indicate a low information transfer to neocortex, whereas high level of coupling during REM sleep may be indicative of an information flow out of the hippocampus to the neocortex for long-term storage. Alternatively, one can hypothesize that low gamma coupling favors interregional synchronization, whereas high gamma coupling supports more local synchronization [47, 48]. In partial agreement with this, theta nested gamma oscillations has been hypothesized to provide the basic mechanism for memory retrieval and encoding [49, 50], whereas the occurrence of distinct gamma bands on different theta phases may help to minimize the interference between retrieval and encoding streams [50, 51]. In this context, subicular theta–gamma$_{UH}$ coupling significantly decreased in a

mouse model of Alzheimer's disease [31], which further refers to theta–gamma$_{UH}$ coupling as an indicator of new memory formation. Further investigations are required to experimentally test this hypothesis.

Consistent with a possible role of phase–amplitude coupling in memory processing during wakefulness [14, 16, 22], we found that theta–gamma coupling, theta phase coherence, and theta power are strongly decreased during optogenetic silencing of MS^{GABA} neurons (~75%, ~40%, ~55%, respectively), whereas gamma power remained nearly unaltered (~10% reduction). Interestingly, our previous study showed that this optogenetic perturbation completely blocks the consolidation of contextual memory during REM sleep [3]. Thus, a possible mechanistic interpretation of this latter finding is that MS^{GABA} neuron projections to the hippocampus contribute to the modulation of theta–gamma coupling and theta phase coherence during REM sleep, both of which have been shown to be essential for proper short-term [52] or working [53, 54] memory formation and long-term memory formation (e.g. spike-timing-dependent plasticity) [47, 48, 53, 55, 56]. However, this link remains correlative at this point and awaits further investigations as other extrinsic, or intrinsic, inputs modulating theta–gamma coupling in the hippocampus may exist.

Finally, the synchronization of circuit oscillations extended beyond theta–gamma coupling during REM sleep [57, 58]. During NREM sleep, slow waves, spindles, and hippocampal sharp wave-ripples (SWRs) are temporally coupled, a mechanism thought to facilitate hippocampal–neocortical transfer during sleep-dependent memory consolidation [57–61]. Hippocampal SWRs involve cycles of 50–150 ms bursting spikes, which propagate along the CA3-CA1-subiculum axis [62]. They are associated with the replay of place cells and synaptic activities critical for the encoding of space/context/time [63–65].

Coupling between ripples and spindles in human has been previously reported in hippocampal [66] and para-hippocampal sites [57]. Consistent with previous observations in rodents [67], monkeys [68], and humans [66], our findings show that hippocampal ripples are also phase-locked to both spindles and slow oscillations within the subiculum in mice, although for CA3 and CA1 recording sites ripples were only coupled to sharp waves (Supplementary Figure 3). The coordination of spindles with ripple oscillations in the subiculum is consistent with a possible mechanism mediating hippocampal–neocortical dialog during NREM sleep [44, 58]. How these phenomena during NREM sleep relate to theta–gamma coupling, or theta coherence, during REM sleep and the overall memory consolidation remains unclear. They may represent distinct, but complementary, pathways for the consolidation of different types of memories, although this awaits further investigation.

Transition between wake, NREM and REM sleep are relatively slow (i.e. several seconds) and implicate many different cell types including neurons and glia. Further insights in the temporal and spatial dynamics of brain-wide distributed network controlling those states will refine the transitions between states. In this context, MI represents an additional criterion to define REM sleep from either its onset from NREM or its termination by wakefulness in rodents, as well as NREM in human. Consistent with the region-specific regulation of sleep oscillations during NREM [9, 69] and REM [70] sleep, our findings further extend the identification of region-specific coupling of oscillatory networks during REM sleep. Our results also emphasize the spatiotemporal dynamic modulation of neural network activity within single REM sleep episode and its possible implication in sleep-dependent functions.

Supplementary material

Supplementary material is available at *SLEEP* online.

Funding

Acknowledgments

Disclosure

The authors declare no competing financial interests.

References

1. Wilson MA, *et al*. Reactivation of hippocampal ensemble memories during sleep. *Science*. 1994;**265**(5172):676–679.

2. Siegel JM. The REM sleep-memory consolidation hypothesis. *Science*. 2001;**294**(5544):1058–1063.

3. Boyce R, *et al*. Causal evidence for the role of REM sleep theta rhythm in contextual memory consolidation. *Science*. 2016;**352**(6287):812–816.

4. Tononi G, *et al*. Sleep and the price of plasticity: from synaptic and cellular homeostasis to memory consolidation and integration. *Neuron*. 2014;**81**(1):12–34.

5. Lee ML, *et al*. Fragmentation of rapid eye movement and nonrapid eye movement sleep without total sleep loss impairs hippocampus-dependent fear memory consolidation. *Sleep*. 2016;**39**(11):2021–2031.

6. Stickgold R, *et al*. Sleep, learning, and dreams: off-line memory reprocessing. *Science*. 2001;**294**(5544):1052–1057.

7. Fraize N, *et al*. Levels of interference in long and short-term memory differentially modulate non-REM and REM sleep. *Sleep*. 2016;**39**(12):2173–2188.

8. Nadasdy Z, *et al*. Replay and time compression of recurring spike sequences in the hippocampus. *J Neurosci*. 1999;**19**(21):9497–9507.

9. Huber R, *et al*. Local sleep and learning. *Nature*. 2004;**430**(6995):78–81.

10. Aeschbach D, *et al*. A role for non-rapid-eye-movement sleep homeostasis in perceptual learning. *J Neurosci*. 2008;**28**(11):2766–2772.

11. Leong RLF, Koh SYJ, Chee MWL, Lo JC. Slow wave sleep facilitates spontaneous retrieval in prospective memory. *Sleep*. 2019;42(4), zsz003. doi:10.1093/sleep/zsz003.

12. Scheffer-Teixeira R, *et al*. Theta phase modulates multiple layer-specific oscillations in the CA1 region. *Cereb Cortex*. 2012;**22**(10):2404–2414.

13. Jensen O, *et al*. Cross-frequency coupling between neuronal oscillations. *Trends Cogn Sci*. 2007;**11**(7):267–269.

14. Tort AB, *et al*. Theta-gamma coupling increases during the learning of item-context associations. *Proc Natl Acad Sci USA*. 2009;**106**(49):20942–20947.

15. van Wingerden M, *et al*. Phase-amplitude coupling in rat orbitofrontal cortex discriminates between correct and incorrect decisions during associative learning. *J Neurosci*. 2014;**34**(2):493–505.

16. Axmacher N, *et al*. Cross-frequency coupling supports multi-item working memory in the human hippocampus. *Proc Natl Acad Sci USA*. 2010;**107**(7):3228–3233.

17. Hyafil A, *et al*. Speech encoding by coupled cortical theta and gamma oscillations. *Elife*. 2015;**4**:e06213.

18. Sweeney-Reed CM, *et al*. Corticothalamic phase synchrony and cross-frequency coupling predict human memory formation. *Elife*. 2014;**3**:e05352.

19. Scheffzük C, *et al*. Selective coupling between theta phase and neocortical fast gamma oscillations during REM-sleep in mice. *PLoS One*. 2011;**6**(12):e28489.

20. Schomburg EW, *et al*. Theta phase segregation of input-specific gamma patterns in entorhinal-hippocampal networks. *Neuron*. 2014;**84**(2):470–485.

21. Belluscio MA, *et al*. Cross-frequency phase-phase coupling between θ and γ oscillations in the hippocampus. *J Neurosci*. 2012;**32**(2):423–435.

22. Tort AB, *et al*. Dynamic cross-frequency couplings of local field potential oscillations in rat striatum and hippocampus during performance of a T-maze task. *Proc Natl Acad Sci USA*. 2008;**105**(51):20517–20522.

23. Voloh B, *et al*. Theta-gamma coordination between anterior cingulate and prefrontal cortex indexes correct attention shifts. *Proc Natl Acad Sci USA*. 2015;**112**(27):8457–8462.

24. Takeuchi S, *et al*. Gamma oscillations and their cross-frequency coupling in the primate hippocampus during sleep. *Sleep*. 2015;**38**(7):1085–1091.

25. Cohen MX, *et al*. Oscillatory activity and phase-amplitude coupling in the human medial frontal cortex during decision making. *J Cogn Neurosci*. 2009;**21**(2):390–402.

26. Canolty RT, *et al*. High gamma power is phase-locked to theta oscillations in human neocortex. *Science*. 2006;**313**(5793):1626–1628.

27. Watrous AJ, *et al*. Phase-amplitude coupling supports phase coding in human ECoG. *Elife*. 2015;**4**:e07886.

28. Schroeder CE, *et al*. Low-frequency neuronal oscillations as instruments of sensory selection. *Trends Neurosci*. 2009;**32**(1):9–18.

29. Stefanics G, *et al*. Phase entrainment of human delta oscillations can mediate the effects of expectation on reaction speed. *J Neurosci*. 2010;**30**(41):13578–13585.

30. Zhang X, *et al*. Impaired theta-gamma coupling in APP-deficient mice. *Sci Rep*. 2016;**6**:21948.

31. Goutagny R, *et al*. Alterations in hippocampal network oscillations and theta-gamma coupling arise before Aβ overproduction in a mouse model of Alzheimer's disease. *Eur J Neurosci*. 2013;**37**(12):1896–1902.

32. Barr MS, *et al*. Impaired theta-gamma coupling during working memory performance in schizophrenia. *Schizophr Res*. 2017;**189**:104–110.

33. de Hemptinne C, *et al*. Exaggerated phase-amplitude coupling in the primary motor cortex in Parkinson disease. *Proc Natl Acad Sci USA*. 2013;**110**(12):4780–4785.

34. Canolty RT, *et al*. The functional role of cross-frequency coupling. *Trends Cogn Sci*. 2010;**14**(11):506–515.

35. Jarrard LE. On the role of the hippocampus in learning and memory in the rat. *Behav Neural Biol*. 1993;**60**(1):9–26.

36. Montgomery SM, *et al*. Theta and gamma coordination of hippocampal networks during waking and rapid eye movement sleep. *J Neurosci*. 2008;**28**(26):6731–6741.

37. Buzsáki G. Theta oscillations in the hippocampus. *Neuron*. 2002;**33**(3):325–340.

38. Goutagny R, *et al*. Self-generated theta oscillations in the hippocampus. *Nat Neurosci*. 2009;**12**(12):1491–1493.

39. Amilhon B, *et al*. Parvalbumin interneurons of hippocampus tune population activity at theta frequency. *Neuron*. 2015;**86**(5):1277–1289.

40. Adamantidis AR, *et al*. Neural substrates of awakening probed with optogenetic control of hypocretin neurons. *Nature*. 2007;**450**(7168):420–424.

41. Cohen MX. Assessing transient cross-frequency coupling in EEG data. *J Neurosci Methods*. 2008;**168**(2):494–499.

42. Mormann F, *et al*. Mean phase coherence as a measure for phase synchronization and its application to the EEG of epilepsy patients. *Physica D*. 2000;**144**(3–4):358–369.

43. Helfrich RF, *et al*. Old brains come uncoupled in sleep: slow wave-spindle synchrony, brain atrophy, and forgetting. *Neuron*. 2018;**97**(1):221–230.e4.

44. Diekelmann S, *et al*. The memory function of sleep. *Nat Rev Neurosci*. 2010;**11**(2):114–126.

45. Buzsáki G, *et al*. Mechanisms of gamma oscillations. *Annu Rev Neurosci*. 2012;**35**:203–225.

46. Sirota A, *et al*. Entrainment of neocortical neurons and gamma oscillations by the hippocampal theta rhythm. *Neuron*. 2008;**60**(4):683–697.

47. Fries P. A mechanism for cognitive dynamics: neuronal communication through neuronal coherence. *Trends Cogn Sci*. 2005;**9**(10):474–480.

48. Axmacher N, *et al*. Memory formation by neuronal synchronization. *Brain Res Rev*. 2006;**52**(1):170–182.

49. Colgin LL. Theta-gamma coupling in the entorhinal-hippocampal system. *Curr Opin Neurobiol*. 2015;**31**:45–50.

50. Colgin LL, *et al*. Frequency of gamma oscillations routes flow of information in the hippocampus. *Nature*. 2009;**462**(7271):353–357.

51. Hasselmo ME, *et al*. A proposed function for hippocampal theta rhythm: separate phases of encoding and retrieval enhance reversal of prior learning. *Neural Comput*. 2002;**14**(4):793–817.

52. Lisman JE, *et al*. Storage of 7 +/- 2 short-term memories in oscillatory subcycles. *Science*. 1995;**267**(5203):1512–1515.

53. Fell J, *et al*. The role of phase synchronization in memory processes. *Nat Rev Neurosci*. 2011;**12**(2):105–118.

54. Lisman JE, *et al*. The θ-γ neural code. *Neuron*. 2013;**77**(6):1002–1016.

55. Benchenane K, *et al*. Coherent theta oscillations and re-organization of spike timing in the hippocampal- prefrontal network upon learning. *Neuron*. 2010;**66**(6):921–936.

56. Fries P. Rhythms for cognition: communication through coherence. *Neuron*. 2015;**88**(1):220–235.

57. Clemens Z, *et al*. Temporal coupling of parahippocampal ripples, sleep spindles and slow oscillations in humans. *Brain*. 2007;**130**(Pt 11):2868–2878.

58. Maingret N, *et al*. Hippocampo-cortical coupling mediates memory consolidation during sleep. *Nat Neurosci*. 2016;**19**(7):959–964.

59. Laventure S, *et al*. Beyond spindles: interactions between sleep spindles and boundary frequencies during cued reactivation of motor memory representations. *Sleep*. 2018;**41**(9).

60. Siapas AG, *et al*. Coordinated interactions between hippocampal ripples and cortical spindles during slow-wave sleep. *Neuron*. 1998;**21**(5):1123–1128.

61. Sirota A, *et al*. Communication between neocortex and hippocampus during sleep in rodents. *Proc Natl Acad Sci USA*. 2003;**100**(4):2065–2069.

62. Chrobak JJ, *et al*. High-frequency oscillations in the output networks of the hippocampal-entorhinal axis of the freely behaving rat. *J Neurosci*. 1996;**16**(9):3056–3066.

63. Buzsáki G, *et al*. Cellular bases of hippocampal EEG in the behaving rat. *Brain Res*. 1983;**287**(2):139–171.

64. Girardeau G, *et al*. Selective suppression of hippocampal ripples impairs spatial memory. *Nat Neurosci*. 2009;**12**(10):1222–1223.

65. Axmacher N, *et al*. Ripples in the medial temporal lobe are relevant for human memory consolidation. *Brain*. 2008;**131**(Pt 7):1806–1817.

66. Staresina BP, *et al*. Hierarchical nesting of slow oscillations, spindles and ripples in the human hippocampus during sleep. *Nat Neurosci*. 2015;**18**(11):1679–1686.

67. Latchoumane CV, *et al*. Thalamic spindles promote memory formation during sleep through triple phase-locking of cortical, Thalamic, and Hippocampal rhythms. *Neuron*. 2017;**95**(2):424–435.e6.

68. Takeuchi S, *et al*. Spatiotemporal organization and cross-frequency coupling of sleep spindles in primate cerebral cortex. *Sleep*. 2016;**39**(9):1719–1735.

69. Vyazovskiy VV, *et al*. Local sleep in awake rats. *Nature*. 2011;**472**(7344):443–447.

70. Funk CM, *et al*. Local slow waves in superficial layers of primary cortical areas during REM sleep. *Curr Biol*. 2016;**26**(3):396–403.